Synthesis and Characterization of Dual-Functionalized Laponite Clay for Acrylic Nanocomposites

Junzuo Wang, Paul A. Wheeler, William L. Jarrett, Lon J. Mathias

Department of Polymer Science, The University of Southern Mississippi, Hattiesburg, Mississippi 39406-0076

ABSTRACT: Dual-functional laponites were synthesized by a condensation reaction with silane coupling agents followed by cation exchange reaction with quaternary ammonium salts. FTIR and solid state ^{13}C CP/MAS NMR confirmed their structures. Quantitative solid state ^{29}Si DP/MAS NMR spectra indicated that clay silanol groups reacted with silane coupling agents by a decrease in the silanol peak and appearance of a new Si—O—Si peak. Dual-functionalized laponites showed improved dispersion in organic solvents and vinyl monomers. One dual-functional laponite modified with both photosensitizer and coinitiator photo-initiated polymerization of an acrylate (2-phenoxyethyl acrylate, PEA) and a methacrylate (MHMA, methyl α-hydroxymethylacrylate). TEM showed laponite clay sheets were exfoliated in poly(PEA); while a combination of exfoliated, intercalated and tactoid morphologies was found in poly(methyl α-hydroxymethylacrylate). The other dual-functionalized laponite clay with edge-bound methacrylate units copolymerized with methyl methacrylate and led to a high grafting amount and graft efficiency. PMMA nanocomposites showed higher storage modulus both below and above the glass transition temperature compared to the PMMA control. © 2007 Wiley Periodicals, Inc. J Appl Polym Sci 106: 1496–1506, 2007

Key words: dual-functionalized laponite; clay cation exchange; PMMA nanocomposite; solid state ^{13}C CP/MAS NMR; ^{29}Si DP/MAS NMR; free-radical polymerization; photopolymerization

INTRODUCTION

Polymer-clay nanocomposites have been extensively described in recent years.[1–4] Nanocomposites can increase specific properties of pristine polymers at a lower concentration than conventional reinforcing agents such as glass or carbon fibers. Untreated clay exhibits hydrophilic features while many polymers are hydrophobic, resulting in phase separation upon attempted mixing. Organic modification of clay is the main method to improve dispersion of clays in a polymer matrix. Surface modification usually involves a cation exchange reaction with quaternary ammonium or phosphonium ions while some examples have been reported of complexation of surface sodium ions by poly(ethylene glycol).[1–5] Modifying clay by condensation reaction of inorganic hydroxyl groups with silane agents has also been reported recently, and this involves predominantly free edge Si—OH groups, for example.[6–14] However, there are only a few reports of preparing dual-functional clays by combining the two modification methods.[15–19]

A twice-functionalized organoclay (TFC) was described involving reaction of a silane agent (glycidoxypropyl trimethoxysilane) with C25A, a montmorillonite modified with a quaternary ammonium

Correspondence to: L. J. Mathias (lon.mathias@usm.edu).

salt.[15–18] Polymer nanocomposite compounded with this TFC showed improved elongation at break as well as increased tensile modules and tensile strength.[15–18] Edge functionalized montmorillonite has been obtained by reaction with the ammonium salt of 1-hydroxy-dodecane-1,1-diphosphonate followed by exchange with 110 meq of dimethyldihydrogenated tallow ammonium chloride.[19] An olefinic polymer compounded with the above organoclay showed 300× improvement in barrier properties.- There is only one other report of dual-functionalized laponite clay that we are aware of, and that involved work carried out in our laboratory.[20] Laponite clay was modified with mono-functional silane agent followed by ammonium salt. PMMA was grown from or to laponite clay from edge functional with ATRP initiator or methacrylate. In this article, less expensive trifunctional silane agent was modified clay edge followed by a clay surface modification with ammonium salt. Methacrylate and acrylate was graft from or to laponite clay from edge functional UV initiator or methacrylate.

It has been found that modification of clays with silane agents generally leads to low organic loading. It has also been suggested that a crosslinked network formed on the clay edges involves oligomerization of the trialkoxysilanes with each other and with more than one clay layer. This results in poor dispersion in organic solvents or reactive monomers.[7–10] Similarly, hybrids of SiO$_2$ nanoparticles with organosiloxane in

water led to oligomerization or network formation of the silane agents.[13] Those modified clays do not readily disperse in acrylate monomers and this directly affects the transparency and hardness of obtained coatings. Modifying the clay edge first and then the surface is expected to improve the dispersion of organo-clay in organics and perhaps give better ultimate properties of the nanocomposites formed.

Laponite is a synthetic layered smectite silicate clay with an average diameter of 25 nm and thickness of 0.92 nm. It possesses a nominal chemical formula of $Na_{0.7}\plus[(Si_8Mg_{5.5}Li_{0.3})O_{20}(OH)_4]^{-0.7}$, with a cation exchange capacity of 50–55 mmol/100 g.[21] Readily accessible hydroxyl groups are also present and it is presumed that most of these are located on the edge of the platelets. Compared with montmorillonite (with a thickness of 1 nm and 70–300 nm across), laponite clay has a higher ratio of edge to surface (0.07), making it an ideal candidate for studying combined edge and surface modifications. A variety of reactions were conducted to explore synergism of two types of clay modifiers possessing reactive functional groups. For example, photo-polymerizations initiated with an aromatic ketone show a synergistic effect of photosensitizer and photocoinitiator (in many cases, an electron rich species such as a trialkylamine).[22] Similarly, ATRP (atom transfer radical polymerization) uses a combination of labile halide and metal ligand complex.[23] Combinations of both required functional groups in one clay sheet may provide synergism in applications ranging from nanoreactors to multifunctional nanomaterials and clay-enhanced polymer blends and mixtures. In addition, binding one polymer-reactive functional group to the edge of a clay platelet and another to the surface opens the possibility of having two different polymers chemically attached to the same particle; this could also lead to enhanced blending and physical properties.

In this article, two dual-functionalized laponites were synthesized by first reacting accessible hydroxyl groups with silane agents and then displacing interlayer cations with a quaternary ammonium halide. One dual-functionalized laponite with a photosensitizer and coinitiator was used to initiate photo-polymerization of an acrylate [2-phenoxyethyl acrylate, (PEA)] and a methacrylate (methyl α-hydroxymethylacrylate). The other dual-functionalized laponite with covalently-bound methacrylates was copolymerized with methyl methacrylate (MMA) to form polymer-grafted clay nanocomposite.

EXPERIMENTAL SECTION

Materials

N,N'-dimethylaminopropyltrimethoxysilane (DAPS) and γ-methacryloxypropyltrimethoxysilane (MPTS)

were purchased from Gelest. The clay used was synthetic laponite RD from Southern Clay Products. Methyl α-hydroxymethylacrylate (MHMA) was donated by Nippon Shokubai, Tokyo, Japan, and was purified by silica gel column chromatograph just before use. MMA, PEA, cetyltrimethylammonium bromide (CTAB), triethylamine, 1-bromooctadecane and thionyl chloride were obtained from Aldrich and used without further purification except for MMA which was distilled from CaH_2. DMSO, chloroform, methanol, ethanol (95%), CH_3CN, $MgSO_4$, and sodium bicarbonate were obtained from Fisher Scientific. 4-Benzoylbenzoic acid and N,N'-dimethylaminoethanol were purchased from Acros Chemical.

Characterization

Solution ^1H and ^{13}C NMR spectra were obtained using a Varian Mercury 200 spectrometer operating at 200 MHz for hydrogen and 50 MHz for carbon. Infrared spectra were recorded on an ATI-Mattson Galaxy 5020 FTIR spectrometer. Thermal analyses were performed on a TA instruments SDT 2960, TGA–DTA was carried out at 10°C/min under nitrogen from ambient temperature to 800°C and DSC performed at 10°C/min under nitrogen from ambient temperature to 200°C. Solid-state ^{13}C CP/MAS NMR analyses were performed on a Varian Unity INOVA 400 MHz spectrometer. Samples were sealed in 7.5-mm zirconium rotors and spun 4 kHz. The standard cross-polarization/magic angle spinning (CP/MAS) technique[24] was used with high-power proton decoupling implemented during FID acquisition. In addition, the TOSS technique[25] was implemented to remove spinning sidebands. The acquisition parameters were as follows: a ^1H 90° pulse width of 4.0 μs, cross-polarization contact time of 1 ms, dead time delay of 6.4 μs, and acquisition time of 45 ms. A recycle delay of 3 s between scans was utilized. For quantitative ^{29}Si acquisition, DP/MAS (direct polarization/magic angle spinning) or Bloch decay techniques were used. The ^{29}Si acquisition parameters consisted of a ^{29}Si pulse width of 4 μs, acquisition time of 45 ms, and recycle delay time of 180 s. X-ray diffraction patterns were obtained using a Rigaku Ultima III diffractometer (Ni-filtered Cu Kα radiation, λ = 1.5405 Å) with power of 40 kV and scanning rate of 2°/min from 2° to 20°. Specimens for transmission electron microscopy were prepared by cryo-sectioning the samples at an angle of 4° to the knife and speed of 1.5–3.5 mm/s on a Reichard–Jung Ultracut E microtome. Ultrathin sections (~ 90-nm thick) were placed on copper TEM grids. The sections were viewed using a Zeiss EM 109-T electron microscopy operating at 50 kV. DMA tests were carried out with DMA Q800 with heating rate of
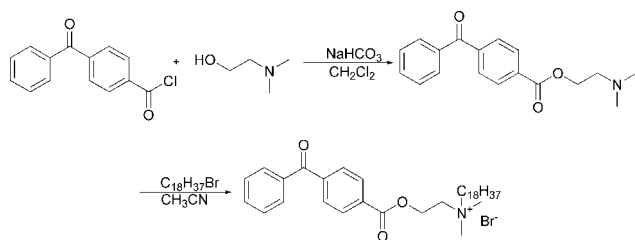
Scheme 1 Synthesis of *N*-2-(4-benzoylbenzoyloxyethyl)-*N*,*N*-dimethyl-*N*-octadecyl ammonium bromide.

2°C/min from 30 to 170°C at 1.00 HZ with a film dimension of $10.0 \times 8.0 \times 0.6$ mm^3.

Synthesis of 2-dimethylaminoethyl-4-benzoylbenzoate.[26,27]

4-Benzoylbenzoyl chloride[6] (0.60 g, 0.0025 mol), sodium bicarbonate (0.23 g, 0.0027 mol), and dichloromethane (10 mL) were charged to a flask with a magnetic stirrer. *N*,*N*′-dimethylaminoethanol (0.88 g, 0.01 mol) mixed with 10-mL dichloromethane was added dropwise to the flask which was cooled in an ice-bath. After addition, stirring was continued overnight. The solid by-product was isolated by vacuum filtration. The dichloromethane solution was extracted with water in a separatory funnel and the dichloromethane layer dried with MgSO$_4$. Dichloromethane was removed with a rotary vaporator to give the product, 2-dimethylaminoethyl-4-benzoylbenzoate (0.46 g, yield: 62.6%).

^{1}H NMR (CDCl$_3$, δ): 8.13 (d, 2H, Ar—*H*), 7.78 (d, 4H, Ar—*H*), 7.58 (m, 1H, Ar—*H*), 7.46 (t, 2H, Ar—*H*), 4.45 (t, 2H, O—C*H*$_2$), 2.74 (t, 2H, C*H*$_2$CH$_2$—N) and 2.34 ppm (s, 6H, C*H*$_3$); ^{13}C NMR (CDCl$_3$, δ): 196.5 (ketone), 166.1 (ester carbonyl); 141.5, 137.1, 133.4, 133.2, 130.3, 130.0, 129.8, 128.7 (aromatic carbons), 63.5 (O—CH$_2$), 57.9 (CH$_2$CH$_2$—N) and 46.0 ppm (N—CH$_3$). The overall synthesis is shown in Scheme 1 below.

Synthesis of *N*-2-(4-benzoylbenzoyloxyethyl)-*N*,*N*-dimethyl-*N*-octadecyl-ammonium bromide

2-Dimethylaminoethyl-4-benzoylbenzoate (0.40 g, 0.0013 mol), 1-bromooctadecane (0.67 g, 0.002 mol) and 12 mL dried CH$_3$CN were charged to a flask with a magnetic stirrer. The system was refluxed overnight. The reaction solution was added to ethyl ether, and the solid product was filtered and washed with ethyl ether. The product was dried at 50°C in a vacuum oven overnight to give *N*-2-(4-benzoylbenzoyloxyethyl)-*N*,*N*-dimethyl-*N*-octadecyl-ammonium bromide (BDOAB) (0.65 g, yield: 77.0%, mp, 121–125°C).

^{1}H NMR (CDCl$_3$, δ): 8.15 (d, 2H, Ar—*H*), 7.81 (d, 4H, Ar—*H*), 7.63 (m, 1H, Ar—*H*), 7.50 (t, 2H, Ar—*H*), 4.94 (t, 2H, O—C*H*$_2$), 4.36 (t, 2H, OCH$_2$C*H*$_2$—N$^+$), 3.70 (t, 2H, CH$_3$(CH$_2$)$_{16}$C*H*$_2$—N$^+$), 3.60 (s, N$^+$—C*H*$_3$), 1.81 ppm (m, 2H, CH$_3$(CH$_2$)$_{15}$C*H*$_2$CH$_2$—N$^+$), 1.25–1.19 (m, 30H, CH$_3$(C*H*$_2$)$_{15}$CH$_2$CH$_2$—N$^+$) and 0.88 ppm (t, 3H, C*H*$_3$(CH$_2$)$_{15}$CH$_2$CH$_2$—N$^+$). ^{13}C NMR (CDCl$_3$, δ): 196.0 (ketone), 165.6 (ester carbonyl), 142.3, 136.7, 133.4, 131.8, 130.4, 130.2, 130.0, 128.7 (aromatic carbons), 65.7 (O—CH$_2$), 62.5 (OCH$_2$CH$_2$—N$^+$), 59.1 (CH$_3$(CH$_2$)$_{16}$CH$_2$—N$^+$), 52.2 (N$^+$—CH$_3$) and 32.2–14.4 ppm (CH$_3$(CH$_2$)$_{16}$CH$_2$—N$^+$).

Synthesis of dual-functionalized laponite 1, Lap-DAPS-BP

Laponite RD (2.96 g), DAPS (2.46 g) and 50-mL dried toluene were charged to a flask equipped with a condenser. The mixture was heated to 110°C and refluxed overnight. After the reaction system was cooled down, the solid was filtered out and washed with toluene four times. The product was dried at 60°C in a vacuum oven for 10 h to give Lap-DAPS (3.42 g). Lap-DAPS (1.2 g) and 48-mL water were put into a flask with a magnetic stirrer. The suspension was kept at 60°C for 1 h and BDOAB (0.84 g) dissolved in a mixture of water and ethanol was added dropwise. After addition, the reaction was continued overnight. The solid product was filtered and washed with a water/ethanol mixture. The product was then dried at 60°C in a vacuum oven for 10 h to give Lap-DAPS-BP (1.43 g).

Synthesis of dual-functionalized laponite 2, Lap-MPTS-CTAB (Scheme 2)

The procedure was similar to the synthesis of Lap-DAPS-BP except the first step was conducted with MPTS at room temperature for 3 days with triethylamine as catalyst,[8,9] and CTAB was used instead of BDOAB in the second step.

Photopolymerization of MHMA and PEA Initiated by Lap-DAPS-BP

MHMA (1.16 g, 0.01 mol) or PEA (1.92 g, 0.01 mol) mixed with Lap-DAPS-BP (0.13 g, 5×10^{-5} mol of benzophenone) was stirred for 1 h and then ultrasonicated for 15 min. The suspension was charged into an aluminum container covered with transparent PP film and purged with nitrogen. A BLAK-RAY long wavelength ultraviolet lamp, MODEL B-100A, was used to irradiate the suspension at a distance of 8 cm from the sample surface for 2.5 h for MHMA and 1.5 h for PEA.
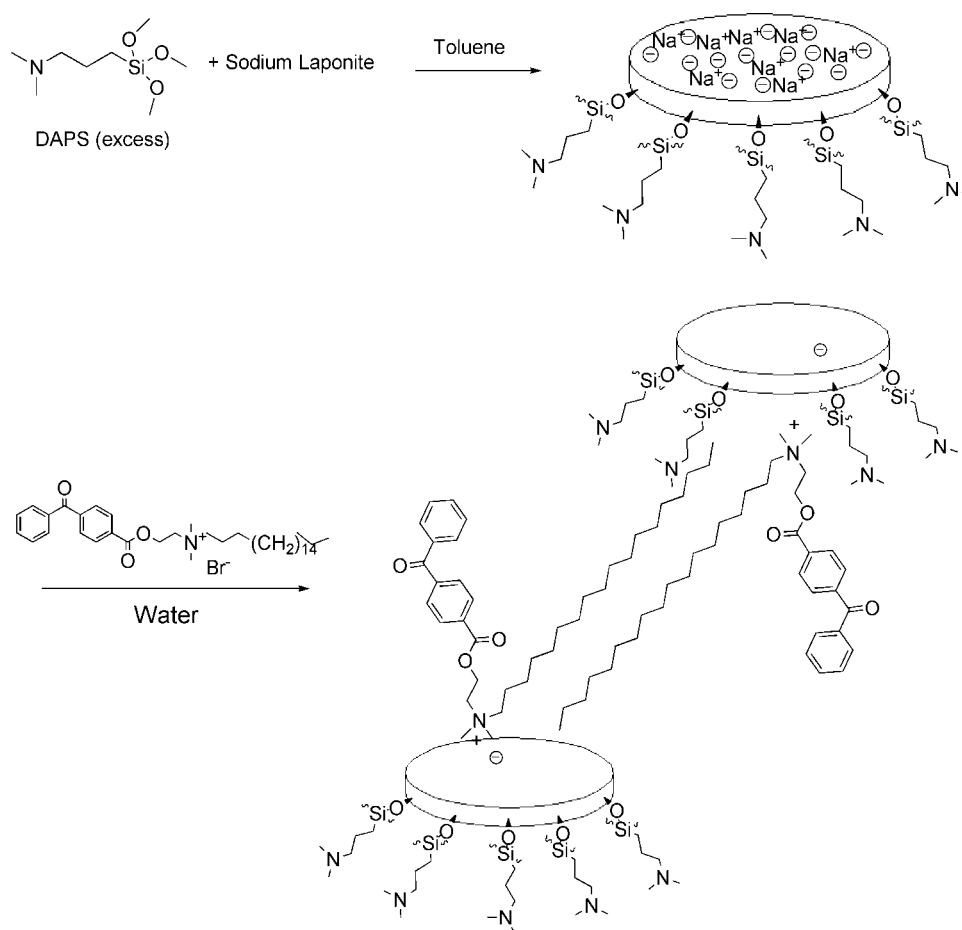
Scheme 2 Schematic representation of the procedure for dual-functionalized laponite clay.

Free radical polymerization of MMA with Lap-MPTS-CTAB

Lap-MPTS-CTAB (2.63 g), MMA (21.6 g), AIBN (0.35 g) and DMSO (24 g) were charged to a 250 mL round flask with a magnetic stirrer. Nitrogen was purged for 20 min and the flask was sealed with a septum. Polymerization was conducted at 70°C for 17 h and a solid polymer hybrid was obtained. The polymer hybrid was dispersed in chloroform and then precipitated into methanol. The solid product was vacuum filtered, washed with methanol, and dried at 60°C in a vacuum oven to give the PMMA nanocomposite (20.1 g, 83% yield). This nanocomposite (7.65 g) was Soxhlet extracted with THF for 24 h to give laponite-bound polymer (4.22 g, yield 46%) and free PMMA (the THF solution was precipitated into methanol to give free PMMA; 2.54 g, yield 28%).

RESULTS AND DISCUSSION

Synthesis of dual-functionalized laponites

The laponite clay structure overall consists of octahedral magnesium ions sandwiched between two layers of tetrahedral silicon atoms linked with oxygen to each other and the central layer. Magnesium is partially replaced by lithium ions to create a net negative charge within the inner layer which is compensated for by surface-bound exchangeable sodium ions.[8,9,21] The silicon and magnesium atoms are connected to a total of twenty oxygen atoms and four hydroxyl groups. There also exists silanol groups (mostly located at the edges)[8–10,28] that, combined with the interlayer exchangeable sodium ions of pristine laponite, allows two kinds of modifications.

Methoxy-containing silane agents such as DAPS and MPTS can condense with hydroxyl groups of laponite clay with varying success, depending on solvent, temperature, and pH value.[29] In the presence of water, silane agents hydrolyze and then condense with themselves to give siloxane oligomers whose silanol groups form hydrogen bonds with the hydroxyl groups of clay to physically absorb on the platelets. Siloxane bonds are then formed with the loss of water during further reaction or drying. When the treatment is carried out in toluene instead, oligomerization of silane agents is decreased, but can not be avoided because of ~ 10% water physically absorbed on pure laponite (as
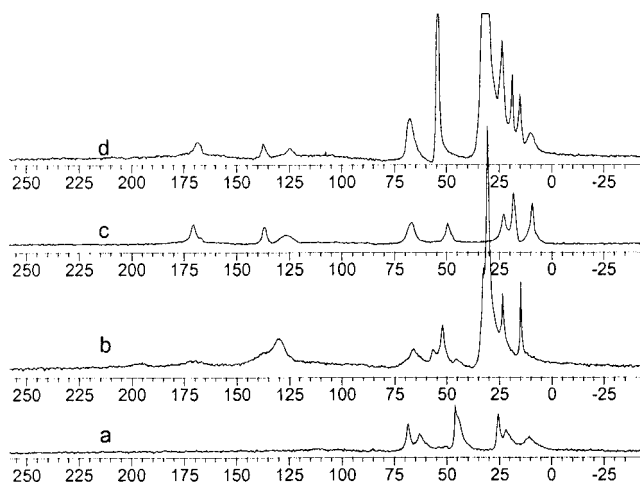
Figure 1 Solid state ^{13}C CP/MAS NMR for dual-functionalized laponite clays: (a) Lap-DAPS, (b) Lap-DAPS-BP, (c) Lap-MPTS, (d) Lap-MPTS-CTAB.

confirmed by TGA). In addition, temperature also aids this process. For example, the methoxy carbon, observed at 50 ppm in the solid state ^{13}C CP/MAS NMR spectrum (spectrum *c* in Fig. 1), appears when the reaction is carried out at room temperature for Lap-MPTS, but nearly disappears when the reaction temperature is 110°C for preparing Lap-DAPS (spectrum *a* in Fig. 1). Unreacted methoxy groups in the clay-bound silanes may hydrolyze in the presence of water and improve the dispersion of the edge-functionalized laponite in water, making cation exchange reaction on the clay interlayers easier. The cation exchange reaction is complete in 12 h at 60°C as confirmed by TGA results discussed below.

Characterization of dual-functionalized laponites

Figure 2 shows FTIR spectra for two kinds of dual-functionalized laponites. Absorbances at 2980, 2890, and 2820 cm^{-1} in the spectrum *a* for Lap-DAPS are the characteristic vibrations of the methylene and methyl groups, respectively, while the 1655 cm^{-1} peak is due to physisorbed water. After Lap-DAPS reacts with BDOAB, peaks at 2930 and 2860 cm^{-1} in spectrum *b* significantly increase because of long alkyl chain incorporation. In addition, peaks at 1720 and 1660 cm^{-1} are characteristic vibrations of aromatic ester and ketone groups associated with the benzophenone moiety. Spectrum *c* for Lap-MPTS exhibits peaks at 2980 and 2910 cm^{-1} related to methylene and methyl groups, respectively. Carbonyl and double bond vibrations are observed at 1720 and 1640 cm^{-1}.[8,9] After Lap-MPTS reacts with CTAB, peaks at 2930 and 2860 cm^{-1} in spectrum *d* (for Lap-MPTS-CTAB) were significantly enhanced

because of incorporation of more methylene and methyl groups, while the carbonyl and double bond vibrations shown at 1720 and 1640 cm^{-1} remain intact.

Table I shows the TGA data for dual-functionalized laponites. In the first step of the condensation reaction, there are 7.3 and 6.0% organic content for Lap-DAPS and Lap-MPTS, respectively, corresponding to condensation capacities (meq of organics/100 g clay) of 48 and 32 meq/100 g. These are 3–4 times higher than that for modification with monoalkoxysilane, indicating that oligomerization and multilayer formation are occurring in clay modified with the trialkoxysilane.[6,8–10] Modifying the hydroxyl sites leaves the surface sodium cations unreacted, allowing further surface modification. On the basis of TGA data (Table I) of surface organic binding, ∼ 58 meq/100 g of cation exchange capacity (CEC) for Lap-DAPS-BP and 56 meq/100 g of CEC for Lap-MPTS-CTAB were achieved. This is in agreement with a reported CEC (50–55 meq/100 g) for pure laponite RD,[21] although there might have been some over-estimation from TGA analysis due to possible surfactant multilayer formation.

Figure 3 shows quantitative solid state DP/MAS ^{29}Si NMR spectra for pristine laponite and Lap-MPTS. The peak at −94.8 ppm is assigned to the Si*(OMg)(OSi)$_3$, a Q$_3$ structure with silicon connected to three tetrahedal silicons.[30] The resonance at −84.7 ppm corresponds to Si*(OMg)(OSi)$_2$(OH), a Q$_2$ structure with silicon connected to two tetrahedal silicons and a free silanol OH that presumably exists on laponite edges. After modification, the intensity of the Q$_2$ peak at −84.7 ppm decreases by 50% (40% for Lap-DAPS) compared to the unmodified laponite. New resonances appearing at −56.1 and −66.1
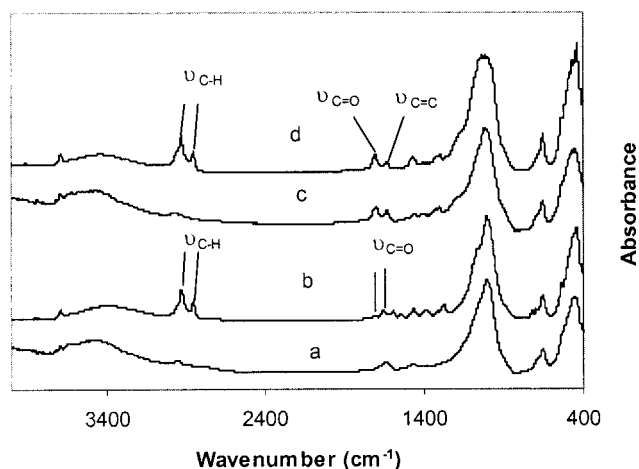
Figure 2 FTIR spectra for dual-functionalized laponite clays: (a) Lap-DAPS, (b) Lap-DAPS-BP, (c) Lap-MPTS, (d) Lap-MPTS-CTAB.

	Lap-DAPS	Lap-DAPS-BP	Lap-MPTS	Lap-MPTS-CTAB
Organic binding (% mass, from 200 to 500 °C)	7.3	28.9	6.0	18.7

ppm were assigned to newly-incorporated T_2 and T_3 structures.[8–10]

Solid state ^{13}C CP/MAS NMR provides additional information about the composition of these hybrid structures (Fig. 1). Spectrum *a* in Figure 1 shows four peaks around 11, 20, 44, and 62 ppm, indicating four kinds of carbons in Lap-DAPS other than methoxy carbons. Disappearance of the methoxy resonance peak around 50 ppm suggests complete condensation with accessible hydroxyl groups of clays and polysiloxane oligomer formation after hydrolysis because of water on the clay surface. After surface modification with ammonium salt, these peaks remain but with reduced intensity because of the concentration effect of DAPS in Lap-DAPS-BP. The broad peak at 195 ppm in spectrum *b* is related to the aromatic ketone, the peak at 169 ppm corresponds to the ester carbonyl, and resonances at 129 and 137 ppm are associated with aromatic carbons. Spectrum *c* shows an ester carbonyl peak at 171 ppm, double bond peaks around 137 and 126 ppm, a methyl peak at 18 ppm, a methoxy peak at 50 ppm, a methacryloxy peak at 66 ppm and methylene peaks at 23 and 9 ppm.

Compared to the solution ^{13}C NMR spectrum of MPTS, chemical shifts of MPTS-modified laponite changed significantly, especially for the methylene carbons linked to silicon which moved from 6 to 9 ppm, indicative of a covalent Si—O bond attachment to laponite clay. After surface modification with CTAB, the methoxy carbon resonance peak disappears because of hydrolysis by water. Peaks still are observed for the ester carbonyl, double bond, and methylene carbons, but their chemical shifts change by 1–2 ppm, suggesting a change in the chemical environment after surface modification. Peaks at 54, 31, 23, 19, and 15 ppm are attributed to CTAB.

Photopolymerization initiated by dual-functionalized laponite

Modification of clays with silane agents generally leads to low organic grafting and linkage of clay sheets by polysiloxane because of condensation of trialkoxysilanes.[8–10] This results in poor dispersion in organic solvents or reactive monomers, and further surface modification is expected to improve the dispersion of organo-clay in organics. This is demonstrated by the results obtained here. Edge functionalized Lap-DAPS does not disperse in MHMA or PEA. However, dual-functionalized Lap-DAPS-BP disperses in both monomers and the suspension of Lap-DAPS-BP in PEA was almost transparent.

Polymerization by UV light offers broad applications in the coating industry because of its efficiency and environmental friendliness. Benzophenone derivatives are often used as photosensitizers along with coreagents that can donate a hydrogen atom, such as tertiary amines, alcohols, ethers, or thiols. In dual-functionalized Lap-DAPS-BP, the benzophenone photosensitizer located within the interlayers of clay is excited upon absorbing UV energy and reacts with tertiary amines located on the clay edges. Only benzophenone located close to the edge-bound DAPS can readily achieve reaction. The slow curing process for MHMA with dual-functionalized Lap-DAPS-BP (2.5 h vs. 15 min with benzophenone and tertiary amine) and PEA (1.5 h vs. 5 min with benzophenone and tertiary amine) is probably due to the restricted movement of the bound reagents. In addition, slow diffusion of clay-bound initiators, or high local concentration of radicals causing self-quenching might also contribute to a slow photopolymerization. Control experiments of pure MHMA and PEA photoirradiated with UV lamp for 2.5 and 1.5 h, respectively, did not show any polymer formation.
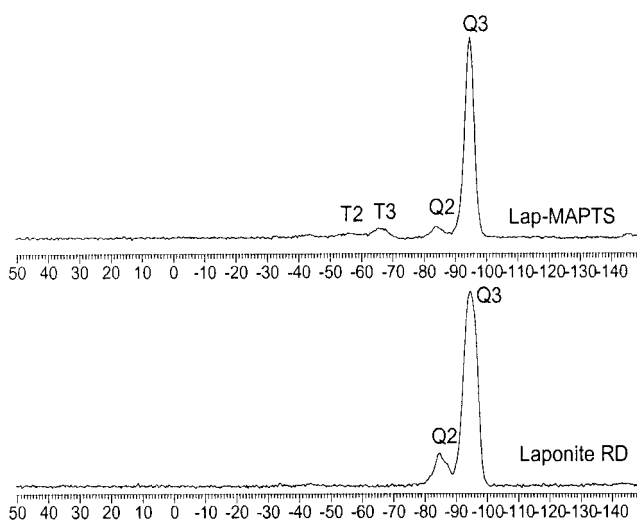
Figure 3 DP/MAS ^{29}Si NMR spectra for laponite RD and MPTS-modified laponite clay.
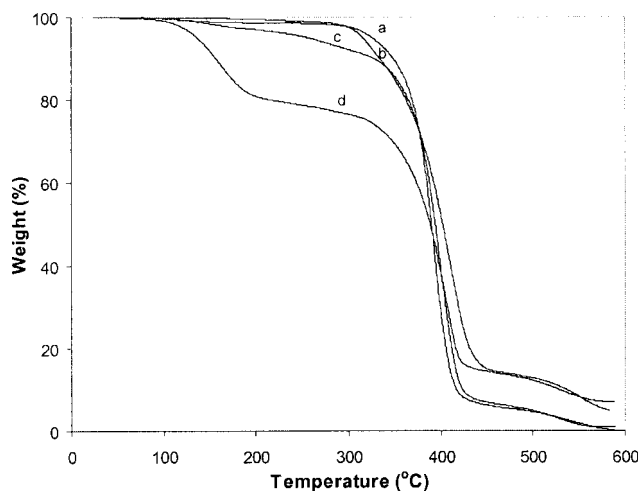
Figure 4 TGA plots for PPEA (initiated with DAPS plus BDOAB) and PPEA nanocomposite (initiated with Lap-DAPS-BP): (a) PPEA after extraction, (b) PPEA nanocomposite after extraction, (c) PPEA before extraction, (d) PPEA nanocomposite before extraction.

Glass transition temperatures (from DSC) for photocured MHMA and PEA initiated with Lap-DAPS-BP are 129 and 12°C, respectively. Photocured MHMA and PEA initiated with a mixture of DAPS and BDOAB for 2.5 and 1.5 h show lower glass transition temperatures of 105° and −5°C, respectively.[31] A possible explanation is that unreacted monomer trapped in polymer or polymer nanocomposite acts as plasticizer and thus lowers the glass transition temperatures.

Photocured MHMA and PEA polymers initiated with benzophenone/tertiary-amine are insoluble in chloroform, indicating crosslink formation because of multiple radical formation by the edge-bound tertiary amines. Figure 4 shows TGA plots of photocured PEA initiated with Lap-DAPS-BP or DAPS plus BDOAB before and after chloroform extraction. There is more unreactive monomer (weight loss from 120 to 300°C) in the PPEA nanocomposite than in pure PPEA. Extraction with chloroform gives a 68% recovery (an indication of monomer conversion) for PPEA nanocomposite and 87% recovery for PPEA. PPEA extracted with chloroform shows a higher glass transition temperature (listed on Table II) than PPEA obtained from solution polymerization.[31] PPEA nano-

TABLE II
DSC Data for PEA Initiated with Lap-DAPS-BP (PPEA-Lap) or DAPS Plus BDOAB (PPEA) Before and After Extraction

	T_g (°C) before extraction	T_g (°C) after extraction
PPEA	−5	10
PPEA-Lap	12	14
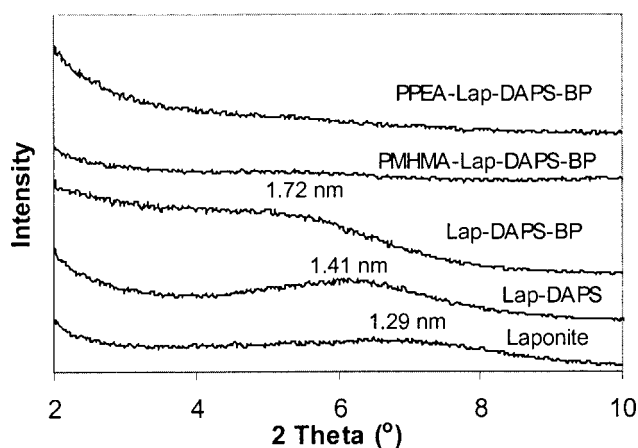
Figure 5 X-ray diffraction curves for sodium laponite, modified laponites and nanocomposites from modified laponites.

composite (7 wt % clay, before and after extraction) shows increased glass transition temperature compared to that without clay.

Figure 5 showed X-ray diffraction patterns for sodium laponite, modified laponites and photo-cured polymer nanocomposites from modified laponites. Sodium laponite shows a broad peak around 6.7° with an interlayer spacing of 12.9 Å. Interlayer spacing of edged-modified laponite was slightly increased to 14.1 Å. After surface modification with intercalated surfactant, interlayer spacing increased from 14.1 to 17.2 Å. In sodium laponite, there inherently exists surface–surface, surface–edge, and edge–edge interaction via ionic, hydrogen bonding, and dipole–dipole interactions, which results in a less ordered layer structure as shown by the broad X-ray diffraction peak. After edge modification, layer structure is improved because of elimination/or decrease of edge–edge and edge–surface interactions. Linking clay sheets together with polysiloxanes from the condensation of trialkoxysilanes may expand clay sheet.[8–10] However, it may also be that there are some polysiloxanes intercalating between the clay sheets. After surface modification, quaternary ammonium salts were clearly intercalated between the clay layers as shown by the absence of X-ray diffraction peaks for PHMMA and PPEA nanocomposites with dual-functionalized laponite. The data suggests disordered structures or interlayer spacings of more than 44 Å.

Figure 6 shows TEM micrographs of sectioned PPEA-Lap-DAPS-BP and PMHMA-Lap-DAPS-BP. At low magnification (left images), clay sheets are uniformly dispersed in PPEA matrix with an average domain size of 200 nm (image c), while PMHMA-Lap-DAPS-BP (image a) shows a relatively poor dispersion with domain sizes ranging from 100 nm to 8 μm. As discussed previously, Lap-DAPS-BP had
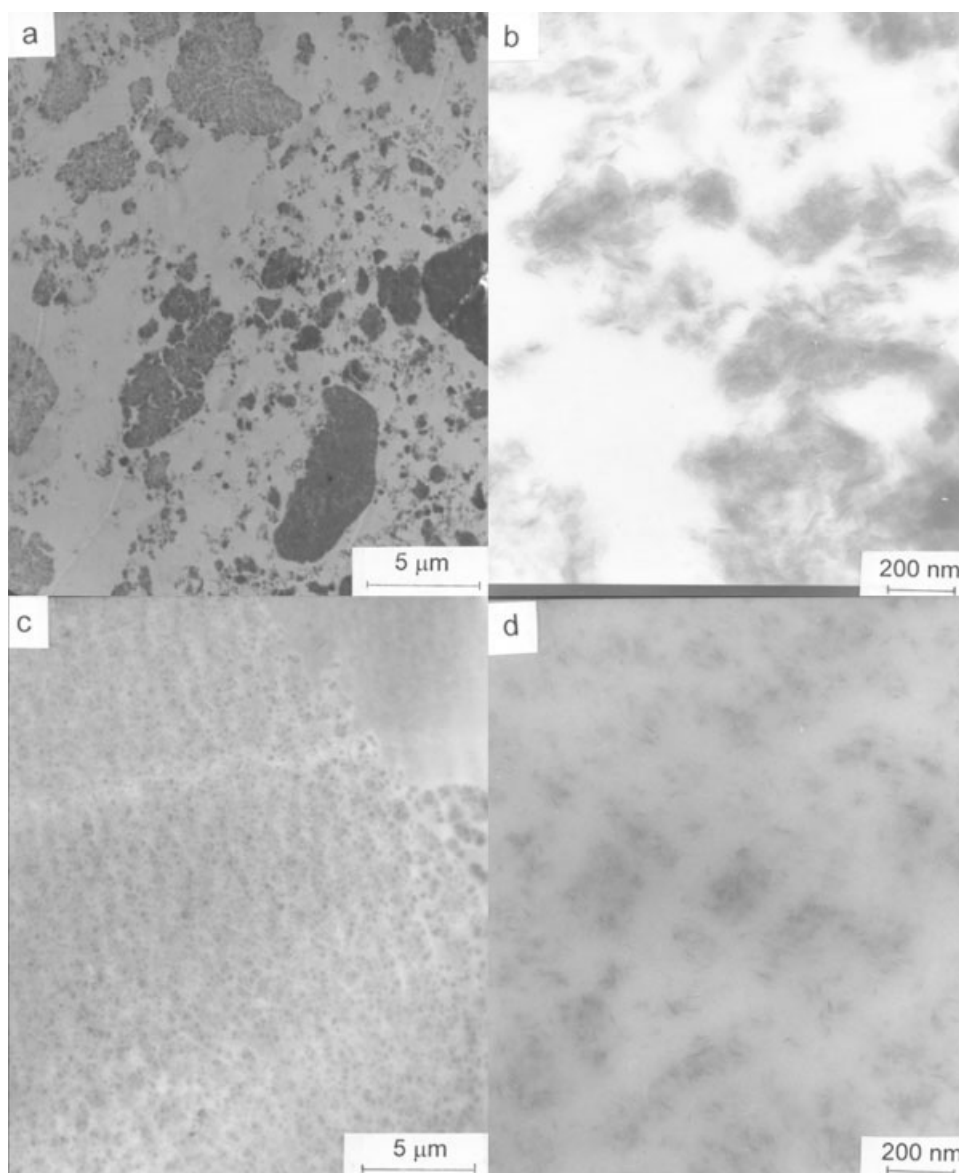
Figure 6 TEM micrographs of PMHMA-Lap-DAPS-BP: (a) Low magnification (3K); (b) High magnification (50K); and PPEA-Lap-DAPS-BP: (c) Low magnification (3K); (d) High magnification (50K).

better dispersion in PEA than in MHMA probably due to a better compatibility of PEA (aromatic compound) with the bound benzophenone groups. In the high magnification image of PMHMA-Lap-DAPS-BP (image *b*), a combination of exfoliation, intercalation and tactoid formation (aggregates of several clay sheets) can be found, while a morphology of combined exfoliation with low tactoid content was observed at high magnification for PPEA-Lap-DAPS-BP (image *d*). Thus, not only is a combination of edge functionalization and surface modification needed to improve the dispersion of laponite clay sheets in a polymer matrix, but also good compatibility of surfactant functional groups with polymer segments is required.

Grafting polymer to dual-functionalized laponite

Reacting polymerizable clay with a vinyl monomer like MMA can allow polymer grafting to a clay core by polymerization through the bound moieties. When Lap-MPTS-CTAB is involved in the free-radical polymerization of MMA, MMA can both homopolymerize and copolymerize with methacryloyl end-groups of bound MPTS.[32] Table III shows the characterization data for PMMA and PMMA nanocomposites.

Copolymerization of MMA with Lap-MPTS-CTAB gave the highest yield of bound polymer (62%). The grafting percentage (polymer weight grafted in g/100 g clay charged) is 300% and graft efficiency

	Nanocomposite clay content[a](%)	T_g/°C[b]	Bound polymer ratio[c] and clay content (%)	T_g/°C	Free poly-mer ratio (%)	T_g/°C	M_n (*10^{-4})	PDI
PMMA					78	108	2.6	1.91
PMMA[d]					98	127	20.3	1.16
PMMA-Lap-MPTS	15.4	122	48.3 and 31.1	126	51.7	121	3.5	2.75
PMMA-Lap-MPTS-CTAB	12.2	122	62.4 and 20.4	128	37.6	123	3.8	1.89

[a] Determined by TGA at 10°C/min at N_2.
[b] Determined by DSC at 10°C/min at N_2.
[c] Ratio of bound polymer in nanocomposite.
[d] MMA polymerized in DMSO with 0.15%-mol AIBN.

(polymer weight grafted in g/100 g polymer) is 50%, which are higher than previous reports.[32,33] Copolymerization of MMA with the Lap-MPTS also gave a high yield (48%) of bound polymer. The grafting amount was 200% and graft efficiency was 37%. Glass transition temperatures of nanocomposites and free polymers all are similar, ranging from 121 to 123°C, while clay bound PMMA shows higher glass transition temperatures. PMMA (obtained with the same polymerization conditions as the PMMA nanocomposites) gave a lower glass transition temperature (108°C) probably due to lower molecular weight. PMMA polymerized with less initiator has a higher molecular weight and higher glass transition temperature. (127°C). Figure 7 gives the TGA curves for PMMA and PMMA nanocomposites. They all show two-stage losses because of the presence of two types of PMMA formed from different radical coupling mechanisms.[34] The onset temperatures for decomposition of the three samples are all similar.

Figure 8 shows X-ray diffraction patterns for laponites and nanocomposites from modified laponites. Sodium laponite gave a broad peak around 6.7°

with an interlayer spacing of 12.9 Å. Interlayer spacing of edged modified laponite was slightly increased to 13.7 Å probably because of linkage of clay sheets with trialkoxysilane oligomers.[8–10] After surface modification with CTAB, interlayer spacing increases from 13.7 to 16.2 Å, consistent with the CTAB laying down between clay sheets with a tilt angle of 5.6° (assuming a bond length for C—C of 1.5 Å). The PMMA nanocomposite with Lap-MPTS shows a broad peak with an interlayer spacing of 18.9 Å suggestive of PMMA interclating between the clay layers. Finally, the PMMA nanocomposite with dual-functionalized laponite possesses a disordered structure with a layer spacing of more than 44 Å.

Figure 9 shows TEM micrographs of sectioned PMMA-Lap-MPTS-CTAB and PMMA-Lap-MPTS. Two separate large domains and four and five smaller domains can be seen for each. PMMA-Lap-MPTS-CTAB displays a slightly better dispersion of clay sheets in the polymer matrix than PMMA-Lap-MPTS as shown by smaller and thinner domains. A combination of well-separated disordered clay sheets and tactoids (aggregates of several clay sheets) is
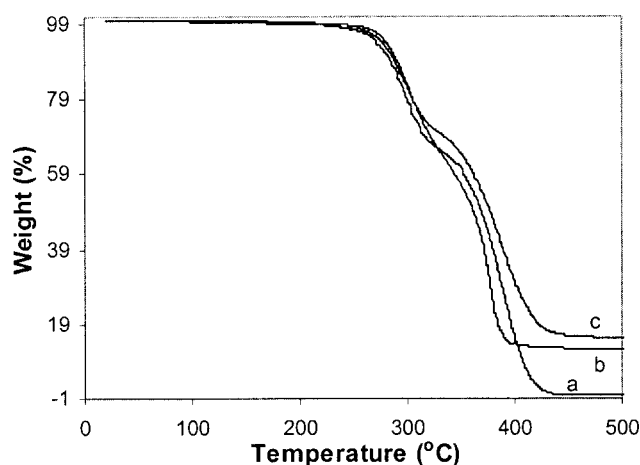
Figure 7 (a) TGA curves for PMMA, (b) PMMA-Lap-MPTS-CTAB and (c) PMMA-Lap-MPTS.
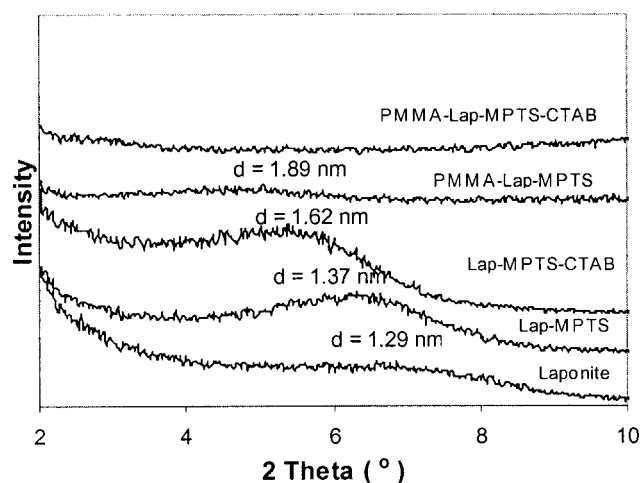
Figure 8 X-ray diffraction patterns for sodium laponite, modified laponites and PMMA nanocomposites from modified laponites.
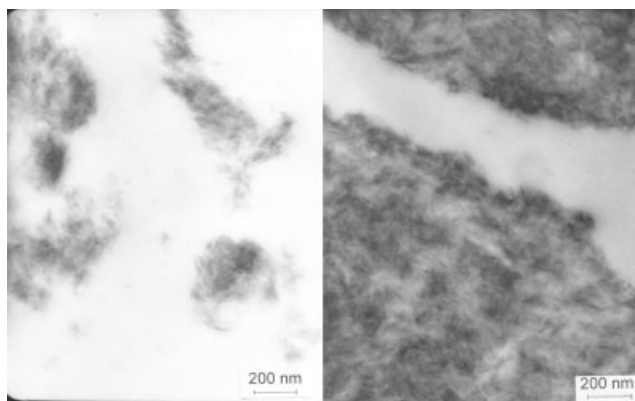
Figure 9 TEM micrographs of PMMA-Lap-MPTS-CTAB (left image) and PMMA-Lap-MPTS (right image).

Figure 11 Images of films (400–600 μm) of PMMA (left one), PMMA-Lap-MPTS-CTAB (middle image), and PMMA-Lap-MPTS (right image). [Color figure can be viewed in the online issue, which is available at www. interscience.wiley.com.]

found in each domain of PMMA-Lap-MPTS. Clay sheets may be linked by trialkoxysilanes and thus polymers grown from them naturally lead to the tactoid morphology shown in both micrographs.[8–10] However, with CTAB intercalation in the clay sheets, polymers penetrate between clay sheets to some extent and improve the dispersion of clay in the polymer matrix, as shown by smaller and thinner domains than without CTAB. Thus, a combination of edge functionalization by monoalkoxysilanes to avoid linkage of clay sheets and surface modification by quaternary ammonium compounds is expected to give the best dispersion of laponite clay sheets in a polymer matrix.

Figure 10 showed DMA curves for PMMA (low and high molecular weight) and PMMA nanocomposites. PMMA nanocomposites both give higher storage moduli at 30°C (below glass transition temperature) and 160°C (above glass transition temperature). Chemical linkages between PMMA and clay by

oligomers of trialkoxysilanes are probably responsible for such increases. Tan δ data show similar trends to the DSC results.

Figure 11 gives representative film images for PMMA, PMMA-Lap-MPTS-CTAB, and PMMA-Lap-MPTS. PMMA-Lap-MPTS-CTAB showed better transparency than PMMA-Lap-MPTS although somewhat less than PMMA.

CONCLUSIONS

Dual-functionalized laponite clays were successfully synthesized by a combination of two combined methods, silanol condensation, and cation exchange reactions. Organ-clay compositions were confirmed by FTIR, solid state ^{13}C CP/MAS NMR and ^{29}Si DP/MAS NMR. A dual-functionalized laponite clay containing a photosensitizer and coinitiator was shown to successfully initiate photopolymerization of an PEA and methyl α-hydroxymethylacrylate although with much slower conversion rates compared to homogenous initiators. Laponite clay sheets were exfoliated in poly(PEA), while a combination of exfoliation, interclation, and tactoid morphology was found in poly(methyl α-hydroxymethylacrylate)/laponite nanocompopsite. The compatibility of clay modifiers with monomers and polymers was probably responsible for this morphology difference. The other dual-functionalized laponite clay with bound methacrylate groups copolymerized with MMA and led to a high grafting amount and graft efficiency. PMMA nanocomposites both showed higher storage modulus, both below and above the glass transition temperature. Overall, dual-functionalized laponites provide a way to improve mechanical properties of PMMA by chemical linkage between PMMA and clay by functional trialkoxysilanes while maintaining

Figure 10 DMA for PMMA and PMMA nanocomposites, (a) storage modulus for PMMA-26k; (a′) tan δ for PMMA-26k; (b) storage modulus for PMMA-Lap-MPTS; (b′) tan δ for PMMA-Lap-MPTS; (c) storage modulus for PMMA-Lap-MPTS-CTAB; (c′) tan δ for PMMA-Lap-MPTS-CTAB; (d) storage modulus for PMMA-203k; (d′) tan δ for PMMA-203k.

transparency of PMMA nanocomposites by using intercalated surfactants.

References

1. Usuki, A.; Kawasumi, M.; Kojima, Y.; Okada, A.; Kurauchi, T.; Kamigaito, O. J Mater Res 1993, 8, 1174.
2. Usuki, A.; Kojima, Y.; Kawasumi, M.; Okada, A.; Fukushima, Y.; Kurauchi, T.; Kamigaito, O. J Mater Res 1993, 8, 1180.
3. Kojima, Y.; Usuki, A.; Kawasumi, M.; Okada, A.; Fukushima, Y.; Kurauchi, T.; Kamigaito, O. J Mater Res 1993, 8, 1185.
4. Kornmann, X.; Berglund, L. A.; Sterte, J.; Giannelis, E. P. Polym Eng Sci 1998, 38, 1351.
5. Lin, J. J.; Chang, Y. C.; Cheng, I. J. Marcomol Rapid Commun 2004, 25, 508.
6. Wang, J.; Wheeler, P. A.; Baker, J. S.; Mathias, L. J. Polym Prepr 2004, 45, 866.
7. Song, K.; Sandi, G. Clays Clay Miner 2001, 49, 119.
8. Herrera, N. N.; Letoffe, J.; Putaux, J.; David, L.; Bourgeat-Lami, E. Langmuir 2004, 20, 1564.
9. Herrera, N. N.; Letoffe, J.; Reymond, J.; Bourgeat-Lami, E. J Mater Chem 2005, 15, 863.
10. Wheeler, P. A.; Wang, J.; Baker, J.; Mathias, L. J. Chem Mater 2005, 17, 3012.
11. Bourlinos, A. B.; Jiang, D. D.; Giannelis, E. P. Chem Mater 2004, 16, 2404.
12. Kazuki, S.; Takeshi, Y.; Koji, S.; Seiji, I.; Masanobu, O. Jpn Pat. 09,002,815 A2 (1997).
13. Tauber, A.; Hartmann, E.; Glasel, H.; Bauer, F.; Mehnert, R. Presented at RadTech, North America, 2002.
14. Zhu, J.; Start, P.; Mauritz, K. A.; Wilkie, C. A. J Polym Sci Part A: Polym Chem 2002, 40, 1498.
15. Chen, G. X.; Yoon, J. S. J Polym Sci Part B: Polym Phys 2005, 43, 478.
16. Chen, G. X.; Choi, J. B.; Yoon, J. S. Macromol Rapid Commun 2005, 26, 183.
17. Chen, G. X.; Kim, H. S.; Shim, J. H.; Yoon, J. S. Macromolecules 2005, 38, 3738.
18. Chen, G. X.; Yoon, J. S. Macromol Rapid Commun 2005, 26, 899.
19. Chaiko, D. J.; Leyva, A. A. Chem Mater 2005, 17, 13.
20. Wheeler, P. A.; Wang, J.; Mathias, L. J. Chem Mater 2006, 18, 3937.
21. Available at: www.laponite.com. Accessed on December 8, 2006.
22. George, B.; Dhamodharan, R. Polym Int 2001, 50, 897.
23. Matyjaszewski, K.; Xia, J. Chem Rev 2001, 101, 2921.
24. Schaefer, J.; Stejskal, E. O.; Buchdahl, R. Macromolecules 1977, 10, 384.
25. Dixon, W. T. J Chem Phys 1982, 77, 1800.
26. Wagner, P. J.; Siebert, E. J. J Am Chem Soc 1981, 103, 7335.
27. Photis, J. A.; Via, F. A. U.S. Pat. 4,080,275 (1978).
28. Mandair, A. P. S.; Michael, P. J.; McWhinnie, W. R. Polyhedron 1990, 9, 517.
29. Arkles, B. CHEMTECH 1977, 7, 766.
30. Carrado, K. A.; Xu, L.; Csencsits, R.; Muntean, J. V. Chem Mater 2001, 13, 3766.
31. Bouchaour, T.; Benmouna, F.; Roussel, F.; Buisine, J. M.; Coqueret, X.; Benmouna, M.; Maschke, U. Polymer 2001, 42, 1663.
32. Bourgeat-Lami, E.; Lang, J. J Colloid Interface Sci 1998, 197, 293.
33. Tsubokawa, N.; Kimoto, T.; Koyama, K. Colloid Polym Sci 1993, 271, 940.
34. Cacioli, P.; Moad, G.; Rizzardo, E.; Serelis, A. K.; Solomon, D. H. Polym Bull 1984, 11, 325.